

Optical reconstruction of digital holograms recorded at 10.6 μm : route for 3D imaging at long infrared wavelengths

Melania Paturzo,* Anna Pelagotti, Andrea Finizio, Lisa Miccio, Massimiliano Locatelli, Andrea Gertrude, Pasquale Poggi, Riccardo Meucci, and Pietro Ferraro

Consiglio Nazionale delle Ricerche-Istituto Nazionale di Ottica Via Campi Flegrei 34,
80078 Napoli and Largo Fermi 6, 50125 Firenze, Italy

*Corresponding author: melania.paturzo@ino.it

Received March 17, 2010; revised May 24, 2010; accepted May 25, 2010;
posted June 2, 2010 (Doc. ID 125652); published June 14, 2010

We demonstrate the optical reconstruction in the visible range (0.532 μm) of digital holograms recorded at long IR wavelengths (10.6 μm) by means of a spatial light modulator. By using an integrated recording-reconstruction system, it is, in fact, feasible to achieve direct imaging of holograms acquired outside the visible range, i.e., in the IR spectrum. By choosing a Fourier recording configuration, the reconstructed image, obtained at about a 20 times shorter wavelength than the acquisition image, exhibits minor aberrations, which do not significantly affect the optical reconstruction. The high NA achievable at a long IR wavelength allows us to image large objects at reasonable distances. © 2010 Optical Society of America

OCIS codes: 090.1995, 090.2870, 110.3080.

Recording holograms using IR wavelengths was judged, since the early stage of holography, as an important goal, considering that this spectral range could open new and interesting perspectives [1–8]. The use of long IR wavelengths reduces the sensitivity of interferometric measurements, and, therefore, IR holography is well suited for measuring optical path variations, avoiding multiple wavelengths methods needed in the visible region [9,10]; moreover, it gives advantages in terms of a larger field of view and less sensitivity to seismic noise, when compared to the visible spectrum. In digital holography (DH), CCD and complementary metal-oxide semiconductor image sensors replace classical photographic plates in the visible range and up to about 1.1 μm [11–13]. Recently, long-wavelength IR radiation image sensors, such as pyrocameras and focal plane array microbolometers, became available with more than 300,000 active pixels and a pixel size down to 25 μm with no need of cryogenic cooling, thus stimulating further studies for DH in this radiation range [14,15]. This renewed interest could have applications in security screening, night vision, and biological science, as it extends holographic 3D imaging capabilities from visible to far IR, toward the terahertz region [16].

Here we demonstrate that efficient and reliable reconstruction in the visible range, of digital holograms recorded with a long IR wavelength, can be accomplished by suitably operating a spatial light modulator (SLM) [17–19], therefore offering the possibility of obtaining, in principle, direct 3D vision at long IR in real time. Secondly, we aim at showing how long IR is a viable route to record digital holograms of large objects and human-size scenes, thanks to the high NA achievable by the present technology at long IR wavelength. As a test object, we used a bronze reproduction of the Benvenuto Cellini “Perseus” sculpture, which resides today at the Loggia dei Lanzi in Florence, Italy. The statuette is about 33 cm in height [Fig. 1(a)]. The setup for the recording and reconstruction process is shown in Fig. 1(b). For a coherent light source, we used a 110 W–CWCO₂ laser, emitting at 10.6 μm . The

laser beam was set on the fundamental TEM₀₀ mode; we took on only a fraction (30 W) of the full power. In these conditions, the laser beam is characterized by a waist of 10 mm and a divergence of 2 mrad. The hologram was acquired by means of an ASi thermal camera (Miracle, Thermoteknix 307 k) with 640 × 480 pixels with 25 μm pixel pitch, without the camera lens. The fringe spacing P was adjusted in order to satisfy the Whittaker–Shannon sampling theorem. From the minimum value of

$$P_{\min} = \frac{\lambda}{2 \sin \frac{\theta_{\max}}{2}} = 2d_p,$$

where λ is the used wavelength, d_p is the pixel pitch, and θ_{\max} is the maximum angle between the reference and the object beam, we can assess the minimum distance $z_{o \min}$ between the object and the detector:

$$z_{o \min} = \frac{D + Nd_p}{2\theta_{\max}} = \frac{d_p(D + Nd_p)}{\lambda} \stackrel{D \gg Nd_p}{\approx} \frac{d_p D}{\lambda}, \quad (1)$$

where D is the object lateral size and N is the number of sensor pixels. Its value is in inverse proportion to the used wavelength λ and in direct proportion to the camera pixel pitch d_p and to the object linear dimension D . Equation (1) points out the advantages of using longer wavelengths,

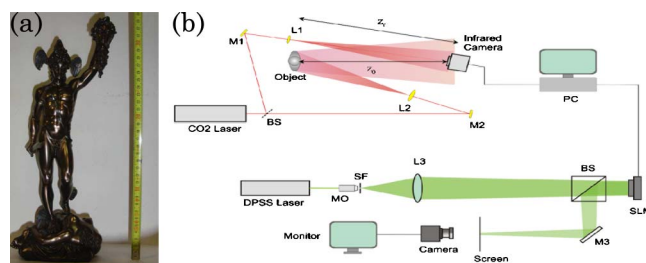


Fig. 1. (Color online) (a) Photo of the Perseus statue. (b) Experimental setup for the recording and reconstruction processes: M, mirror; L, lens; BS, beam splitter; MO, microscope objective; SLM, spatial light modulator; SF, spatial filter.

because the distance between the camera and the object can be reduced to reasonable values, even for large objects. In our case, the recording distance $z_{o\min}$ was 80 cm, corresponding to a lateral maximum recording dimension D of about 34 cm. At the same distance $z_{o\min}$, by using a $\lambda = 0.532 \mu\text{m}$ laser and adopting the available lower pixel size CCD (d_p about $5 \mu\text{m}$) from Eq. (1), the maximum achievable size of the object D results to be only about 8.5 cm. In the reconstruction process, we used a DPSS laser emitting at $0.532 \mu\text{m}$. The laser beam was expanded in such a way as to obtain a converging beam impinging on a liquid-crystal-on-silicon (LCOS) SLM (PLUTO, Holoeye— 1920×1080 pixels and 60 Hz refresh rate), that displayed the holograms acquired by the thermocamera with an acquisition rate of 60 frames/s. By rotating Perseus by 3° , we recorded a hologram sequence. Figure 2 (Media 1) shows the reconstructed image of the rotating figurine, of about 30 cm height, produced on a screen at a distance of 459 cm from the SLM. (Because of inadequate computer performance, some frame displaying failed.) Numerical and optical reconstructions of the holograms sequence were employed to assemble Media 2 and Media 3, respectively. Potential difficulties in this direct reconstruction/visualization method could be caused by the possible aberrations involved. In fact, generally we can state that if a hologram is reconstructed with a wavelength different than the one used in the recording process, the resulting image is affected by some aberrations. In fact, both the magnification of the reconstructed image and the aberrations depend on the wavelength ratio of reconstructing-to-recording light as well as on the scale factor of the hologram. In classical holography, this scaling is obtained through a photographic process [20], while, in this work, it is given by the dissimilar values of the pixel pitch in the recording camera and in the SLM array. However, thanks to the numerical nature of the hologram, it can be properly adjusted to optimize optical reconstruction, if needed. For example, numerical linear and nonlinear stretching can be straightforwardly applied to digital holograms in order to obtain an extended-focus-image of tilted objects and to control focusing in the final image [21]. We used a Fourier



Fig. 2. (Color online) (Media 1) A spectator observing the acquired hologram SLM optical reconstructions, projected on a screen. The size of the image reconstructed at visible wavelength was about 30 cm, comparable to the original object size.

holographic configuration, that according to the Meyer theory [20], allows us to minimize aberrations. Hence, in order to verify that such aberrations do not affect the 3D display, we estimated the aberration coefficients that result from the reconstruction in the visible range of holograms recorded with a wavelength 20 times larger, such as coma, astigmatism, distortion, and curvature of field. Moreover, we calculated the lateral magnification that in the Fourier configuration holography, following the notation of [20], is expressed by the formula $M_{\text{lat}} = \frac{1}{m} \frac{\lambda_c z_i}{\lambda_r z_o}$, where m is the scale factor of the hologram, given by the ratio between the pixel pitch of the SLM and that one of the recording device; λ_r and λ_c are the recording (CO_2 laser = $10.6 \mu\text{m}$) and reconstructing (green laser = $0.532 \mu\text{m}$) wavelengths, respectively, while z_i is the distance between the reconstructed image and the SLM and z_o is that one between the object and the hologram plane. To estimate the magnification, we need to calculate the distance at which the reconstructed image appears in focus. The position of the image is obtained by the formula $\frac{1}{z_i} = \frac{1}{z_c} \pm \frac{1}{m^2} \frac{\lambda_c}{\lambda_r} \left(\frac{1}{z_0} - \frac{1}{z_r} \right)$ where z_r and z_c are the radii of curvature of the reference beam in the recording and reconstruction process, respectively. For a Fourier hologram ($z_o = z_r$), z_i has the same value of the radius of curvature of the reconstructing beam, z_c , and does not depend on the wavelength ratio and on the scale factor of the hologram, m . This is confirmed by the experiment performed in [21], where it is demonstrated that the linear stretching of Fourier holograms does not produce changes in the in-focus reconstruction distance as, instead, it happens for Fresnel holograms.

The parameters used in our experiment, as mentioned above, are $\lambda_r = 10.6 \mu\text{m}$, $\lambda_c = 0.532 \mu\text{m}$, $M = 8/25$, $Z_c = 459 \text{ cm}$, and $z_o = z_r = 80 \text{ cm}$. Therefore, the M_{lat} value is equal to 0.9, in agreement with the measured value [see the scales in Fig. 3]. The reconstruction of a hologram [Fig. 3(b), Media 3], performed at $0.532 \mu\text{m}$, can be compared with the numerical reconstruction, at IR wavelength [Fig. 3(a), Media 2], obtained through the Fourier integral. In the latter case, the zero-order and the twin images are eliminated by applying a high-pass filter and a mask to the hologram Fourier transform, respectively. No evident differences appear, as the two images are scaled up to the same size. This implies that the steps mentioned below do not cause any perceptible distortions, namely: (i) hologram recording at long IR wavelength, (ii) optional numerical preprocessing of digital holograms (i.e., contrast optimization and noise filtering by fast Fourier transform), (iii) reconstruction displaying in the visible range at $0.532 \mu\text{m}$, and (iv) holographic-reconstructed image capturing by a CCD camera. The aim of aberration analysis is an *a priori* evaluation of large distortions eventually affecting the final image. However, adopting the Fourier configuration, the large image distortions are not to be expected and this was confirmed by our experimental data. To estimate the aberration coefficients, we considered the Seidel aberration formula in polar coordinates, ρ and θ . The spherical aberration is zero for holograms acquired in the Fourier configuration, regardless of the magnitude of z_c , λ_r , λ_c , and m [20]. The coma aberration is given by

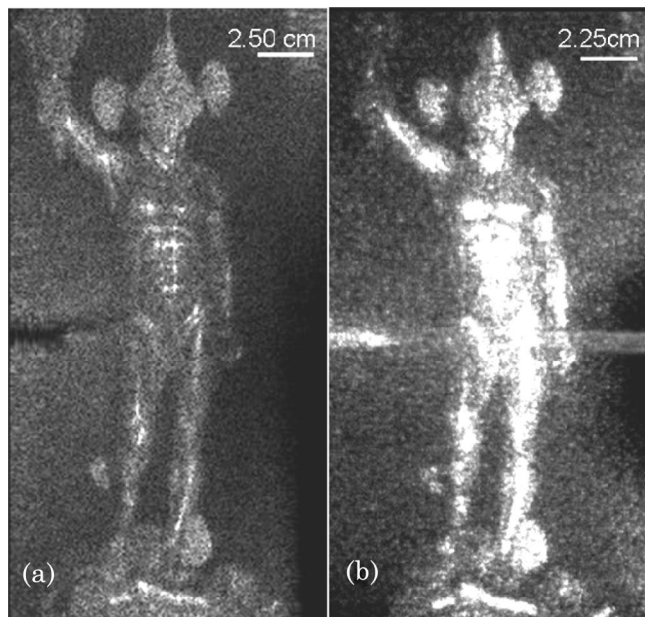


Fig. 3. (a), (Media 2) Numerical reconstruction obtained through the Fourier method. (b), (Media 3) SLM optical reconstruction performed at a visible wavelength.

$$W = \left(\frac{2\pi}{\lambda_c}\right) \left[\frac{1}{2} \rho^3 (C_x \cos \theta + C_y \sin \theta) \right],$$

while the astigmatism is expressed by the formula $W = \left(\frac{2\pi}{\lambda_c}\right) \left[-\frac{1}{2} \rho^2 (A_x \cos^2 \theta + A_y \sin^2 \theta + 2A_{xy} \cos \theta \sin \theta) \right]$.

The field of curvature is given by $W = \left(\frac{2\pi}{\lambda_c}\right) \left[-\frac{1}{4} \rho^2 F \right]$, while the distortion is given by

$$W = \left(\frac{2\pi}{\lambda_c}\right) \left[\frac{1}{2} \rho (D_x \cos \theta + D_y \sin \theta) \right].$$

We computed the aberration coefficients by using the formulas in [20], concerning the holograms acquired in the Fourier configuration. Then, considering that the lateral size of SLM are such that $\rho = 1.5 \text{ mm}$, we have obtained that coma is about $6/1000\lambda$, astigmatism is $5/100\lambda$, field of curvature is $3/100\lambda$, and distortion is $4/10\lambda$, confirming that, in our experimental conditions, the wavefront aberration is negligible (<1 wavelength) and does not substantially affect the reconstructed images, giving the chance of a reliable IR-recording/VIS reconstruction system. Obviously, the displayed image is affected by an unavoidable speckle noise due to the coherence of the light. We intentionally declined to adopt speckle noise reduction strategies [22,23], with the aim of presenting solely the plain result of the optical reconstruction of IR holograms. Moreover, we did not alter the object surface, aiming at demonstrating that the method can be applied to real cultural heritage statues (i.e., made of bronze) in a noninvasive way.

In conclusion, we reported on a system for SLM optical reconstruction, at visible wavelength, of digital holograms acquired in the long IR region ($10.6 \mu\text{m}$). The system demonstrates, for the first time (to the best of our knowledge), through an integrated recording-reconstruction design, the opportunity to achieve direct 3D imaging in far IR region. The presented results pave the way to 3D vision in a spectral region, which may be interesting for many aspects of homeland security and further research in the terahertz range, too.

Funding is provided from the European Community's Seventh Framework Programme FP7/2007-2013 under grant agreement 216105 ("Real 3D" Project).

References

1. D. Prévost, G. Thibault, P. Galarneau, M. Denariez-Roberge, A. Tarrats-Saugnac, and F. de Contencin, *Appl. Opt.* **28**, 3751 (1989).
2. M. Rioux, M. Blanchard, M. Cormier, and R. Beaulieu, *Appl. Opt.* **17**, 3864 (1978).
3. R. Beaulieu, R. A. Lessard, M. Cormier, M. Blanchard, and M. Rioux, *Appl. Opt.* **17**, 3619 (1978).
4. T. Sakusabe and S. Kobayashi, *Jpn. J. Appl. Phys.* **10**, 758 (1971).
5. K. Shigeaki and K. Kyokot, *Appl. Phys. Lett.* **19**, 482 (1971).
6. S. Calixto, *Appl. Opt.* **27**, 1977 (1988).
7. M. Rioux, M. Blanchard, M. Cormier, R. Beaulieu, and D. Bélanger, *Appl. Opt.* **16**, 1876 (1977).
8. G. Decker, H. Herold, and H. Röhr, *Appl. Phys. Lett.* **20**, 490 (1972).
9. J. S. Chivian, R. N. Claytor, and D. D. Eden, *Appl. Phys. Lett.* **15**, 123 (1969).
10. L. Repetto, R. Chittofrati, E. Piano, and C. Pontiggia, *Opt. Commun.* **251**, 44 (2005).
11. P. Ferraro, M. Paturzo, P. Memmolo, and A. Finizio, *Opt. Lett.* **34**, 2787 (2009).
12. P. Ferraro, S. De Nicola, A. Finizio, G. Coppola, S. Grilli, C. Magro, and G. Pierattini, *Appl. Opt.* **42**, 1938 (2003).
13. A. Stadelmaier and J. H. Massig, *Opt. Lett.* **25**, 1630 (2000).
14. N. George, K. Khare, and W. Chi, *Appl. Opt.* **47**, A7 (2008).
15. E. Allaria, S. Brugioni, S. De Nicola, P. Ferraro, S. Grilli, and R. Meucci, *Opt. Commun.* **215**, 257 (2003).
16. Y. Zhang, W. Zhou, X. Wang, Y. Cui, and W. Sun, *Strain* **44**, 380 (2008).
17. M. R. Chatterjee and S. Chen, *Digital Holography and Three-Dimensional Display: Principles and Applications*, T. Poon, ed. (Springer, 2006), Chap. 13, pp. 379–425.
18. C. Kohler, X. Schwab, and W. Osten, *Appl. Opt.* **45**, 960 (2006).
19. O. Matoba, T. J. Naughton, Y. Frauel, N. Bertaux, and B. Javidi, *Appl. Opt.* **41**, 6187 (2002).
20. R. W. Meier, *J. Opt. Soc. Am.* **55**, 1693 (1965).
21. M. Paturzo and P. Ferraro, *Opt. Express* **17**, 20546 (2009).
22. J. Maycock, B. M. Hennelly, J. B. McDonald, Y. Frauel, A. Castro, B. Javidi, and T. J. Naughton, *J. Opt. Soc. Am. A* **24**, 1617 (2007).
23. F. A. Monroy and J. Garcia-Sucerquia, *Opt. Int. J. Light Electron. Opt.*, doi:10.1016/j.ijleo.2009.06.011.